PAPER

Synthesis of fluorescent nitrogen-doped carbon dots from dried shrimps for cell imaging and boldine drug delivery system†‡

Stephanie L. D'souza,[a] Balaji Deshmukh,[b] Jigna R. Bhamore,[a] Karuna A. Rawat,[a] Nibedita Lenka[b] and Suresh Kumar Kailasa*[a]

Fluorescent N-doped carbon dots (CDs) were derived from dried shrimps and rationally fabricated as a traceable drug delivery system for the targeted delivery of boldine to human breast cancer cells (MCF-7 cells). The MCF-7 cells were used to evaluate the anticancer ability of the boldine-loaded CDs. The CDs served as fluorescent carriers that simultaneously tracked and released the drug. The boldine release was triggered upon acidification of the intracellular vesicles, in which the carriers were located after their uptake by cancer cells, and there was further enhancement in the uptake of the boldine-loaded fluorescent CDs by the cancer cells. The synthesized blank CDs were also used as fluorescent probes for the imaging of SH-SY5Y (human neuroblastoma) cells and have potential applications in bioimaging and related fields. These results demonstrate the feasibility of using CDs as a traceable drug delivery system with the ability to deliver boldine drug into the target cells.

Introduction

Cancer, a multifactorial molecular disease that includes the uncontrolled growth and spread of abnormal cells, has taken a tremendous toll on society and causes 1 in 4 deaths in developed countries.[1] It has been reported that 14.1 million new cancer cases were registered worldwide in 2012 and that figure can be expected to increase to over 22 million cases per year in the next two decades.[2] According to the World Health Organization (November 2014), 8.2 million deaths resulted from all cancer types, and 32.6 million people were living with cancer worldwide (within 5 years of diagnosis) in 2012.[3] Drug resistance and the severe side effects of chemotherapy are major unresolved issues in clinical oncology. Novel anticancer compounds with improved features for use in chemotherapy are continuously causing great interest.[4,5] Unregulated cell proliferation and resistance to apoptosis are the key factors responsible for progression in carcinogenesis, which involves multistage processes.[6] Apoptosis (programmed cell death) is the first line of defense in multicellular organisms to stop tumor development, which is characterized by distinct morphological changes, including cell shrinkage, chromatin condensation, membrane permeability, and disruption of the mitochondrial membrane.[7,8] Various organic molecules targeting apoptotic pathways, including camptothecin, paclitaxel, and doxorubicin (DOX), have been exploited as anticancer drugs for cancer therapy as well as chemoprevention.[9] These drugs take effect by regulating key events or molecules in apoptosis-inducing signal transduction pathways. In order to exploit the potential use of plant-derived compounds as drugs, different alkaloid molecules have been isolated from various plants and used as novel anticancer drugs with reduced side effects. Boldine ((*S*)-2,9-dihydroxy-1,10-dimethoxyaporphine) is an aporphine alkaloid found abundantly in *Peumus boldus* Molina[10] It exhibits potent antioxidant activity and possesses hepatoprotective, anti-trypanosomal, and anti-inflammatory properties.[11] As a result, the cytotoxic effects of boldine in bladder carcinoma and glioma cancer cells, as well as its antitumor activity in breast adenocarcinoma, have been studied using *in vitro* and *in vivo* models;[6,12,13] however, boldine delivery studies have not yet been demonstrated.

In recent years, carbon nanomaterial-based drug delivery systems have shown promise in the treatment of cancer due to their capacity for drug loading and release at target cells, which result in better pharmacokinetics and biodistribution of the drug.[14] Among the carbon nanomaterials, carbon dots are a new type of carbon-based nanomaterial recognized as the next generation of green and biocompatible nanomaterials with enormous potential as biocompatible imaging probes due to

[a] Department of Chemistry, S. V. National Institute of Technology, Surat–395007, Gujarat, India. E-mail: sureshkumarchem@gmail.com; skk@ashd.svnit.ac.in; Fax: +91-261-2227334; Tel: +91-261-2201730

[b] National Center for Cell Science, NCCS Complex, Pune University Campus, Pune-411 007, Maharastra, India

† This work is dedicated to Ms Stephanie L. D'souza, who was listed as a First co-author, DST-Inspire Ph.D student in the Department of Applied Chemistry, SVNIT from 2012 to 2015. She passed away on 3rd May 2015 in Ahmedabad, due to heart stroke.

‡ Electronic supplementary information (ESI) available. See DOI: 10.1039/c5ra24621k

their unique optical properties.[15] The surfaces of CDs have different functional groups that can facilitate the attachment of drugs and make them ideal carrier probes for the simultaneous treatment and tracking of cancer cells.[16] In order to enhance the fluorescence properties of CDs, doping with heteroatoms is one promising approach for either enhancing quantum yield or tuning emission wavelength.[17] Among the CD doping elements, nitrogen (N) is the most promising doping atom that can be easily incorporated into the carbon framework, since it has a comparable atomic size and five valence electrons to bind carbon atoms effectively.[18] Various synthetic approaches have been explored to dope nitrogen atoms into the carbon framework using various chemical modifications, such as treatment of carbon materials with ammonia at high temperatures,[19] carbonization of nitrogen containing compounds at high temperature,[20] and polymerization of nitrogen containing compounds in the liquid-phase.[21] In addition, various organic molecules including aminoacids,[22] streptomycin,[23] ethylenediamine tetraaceticacid,[24] mixtures of amines with acid (aniline, ethylene diamine, and phosphoric acid),[25] and various alkanolamines (monoethanolamine, biethanolamine and triethanolamine)[26] have been used as precursors for the doping of heteroatoms (N, S and P) in CDs with enhanced fluorescence, high yield and high biocompatibility. Even though heteroatoms were successfully incorporated into the carbon network, all these above-mentioned methods required either extra chemical additives (precursors) or severe synthetic conditions, which limit their wide applications. Thus, the development of simple and low-cost methods for the incorporation of heteroatoms into the carbon framework is highly desired. This type of doping and functionalization may play a key role in improving the properties of the CDs, which would extend their potential and/or practical applications. To meet green chemistry standards, we selected dried shrimp as precursors for the one-step synthesis of N-doped fluorescent CDs, without any hazardous chemical additives.

In order to explore the potential applications of cell biology, great efforts have been made to develop fluorescent CDs as probes for the imaging of bacteria and cancer cells.[27–30] Tracking of the drug carriers in living cells is another important issue in drug delivery. Mewada and coworkers explored the potential use of sorbitol-derived CDs as drug carriers for the targeted delivery of DOX to cancer cells.[31] Zhou's group functionalized mesoporous silica NPs with CDs and used them as vehicles for delivering DOX.[32] Matai's group described the use of luminescent CDs with anionic termini and cationic acetylated G5 poly(amido amine) dendrimers, for the encapsulation of the chemo-drug epirubicin.[33] The negatively charged fluorescent CDs were synthesized using citric acid and *o*-phenylenediamine as precursors and their anticancer drug delivery was studied *via* electrostatic interactions.[34] A facile green synthetic approach was developed for the preparation of DNA-CDs using genomic DNA isolated from *Escherichia coli*, and their drug delivery imaging properties were investigated.[35] Similarly, Pandey's group functionalized Au NPs with CDs and used them as carriers for delivering DOX under physiological conditions.[36] Karthik's group synthesized a phototrigger conjugated anticancer drug (7-(3-bromopropoxy)-2-quinolylmethyl chlorambucil), and then

loaded it on the N-doped CDs for drug delivery.[37] Song and coworkers illustrated the use of fabricated hyaluronic acid on graphene oxide surfaces for the controlled release of DOX in tumor therapy.[38] Recently, Capelo *et al.* functionalized Au NPs with quinoline for the sensing of mercury ions, and studied their cytotoxicity on the MCF-7 breast cancer cells.[39]

The possibility of using CDs as a drug delivery vehicle to carry the anticancer-therapeutic agent, boldine, is explored in the present study. Herein, we describe a one-step hydrothermal method for the synthesis of N-doped fluorescent CDs, using dried prawns as precursors. The synthesized CDs are used as potential carriers for effective boldine drug delivery, and the toxic effects on cancer cells are studied. To this end, boldine was loaded onto the surfaces of the CDs and the processes of internalization, intracellular distribution, and release were studied. The internalization into vesicles triggered the release of boldine from the CDs, allowing for cell imaging and anticancer drug delivery to MCF-7 cells. The fluorescence of the CDs helped in monitoring the drug release process in the cells.

Experimental section

Chemicals

Dried shrimp was purchased from a local market in Surat. Boldine was procured from Sigma-Aldrich, USA. Dialysis membrane-70 was procured from HiMedia Laboratories Pvt., India. All the chemicals were used as received without further purification. Water used throughout all experiments was obtained using a Milli-Q water system.

Synthesis of CDs, boldine-loading and release from boldine-CDs

The fluorescent CDs were synthesized from dried shrimp through a simple, convenient one-step hydrothermal method. Briefly, 10 g of dried shrimp was placed into 125 mL of EtOH and 125 mL of water, sealed in a Teflon equipped stainless steel autoclave and then placed in a drying oven, followed by hydrothermal treatment at 170 °C for 12 h. After the reaction, the autoclave was cooled to room temperature. The resulting product was dialyzed against distilled water, using a cellulose ester dialysis membrane for 2 days in order to remove impurities from the CDs. A stock solution of boldine (1 mM) was prepared by dissolving 1.6 mg of boldine in 5 mL of EtOH. Different volume ratios of CDs and boldine (10 : 0 and 0 : 10 v/v) were studied for effective molecular assembly of boldine on the surfaces of CDs. The boldine drug loading efficiency of CDs was studied by dialysis of 10 mL boldine-loaded CDs against deionized water at phosphate buffer silane (PBS) pH 5.2, 7.4 and 9.2. The best volume ratios of boldine and CDs were determined using UV-visible spectroscopy. The pH-responsive boldine release behavior was studied using UV-visible and fluorescence spectroscopic techniques. The release of boldine from the CDs at pH 5.2, 7.4 and 9.2 was performed as follows. 7 : 3 mL of boldine-loaded CDs were transferred into a dialysis tube (MWCO ~ 70 kDa), then the tube was immersed into 40 mL of a PBS (pH = 5.2, 7.4 and 9.2) bath at 37 °C. At each time point,

the outer dialysate was collected and replaced with fresh PBS. Samples were collected at intervals of 180 min for 12 h, and then at intervals of 24 h for 3 days. The release of boldine at pH 5.2, 7.4 and 9.2 was analyzed by UV-visible and fluorescence spectroscopic techniques. Cumulative release is expressed as the total percentage of drug released through the dialysis membrane over time using the following formula:

$$[(X_n - X)/X_n] \times 100$$

where X is the fluorescence intensity at 0 hours and X_n is the fluorescence intensity at different hours, *i.e.* X_1, X_2... n for 3, 6, 9... 60 hours.

Cell culture

The cell culture and imaging experiments were carried out at the National Centre for Cell Science, Pune, India. The human breast cancer cell lines (MCF-7) were grown in Dulbecco's modified Eagle's medium (Gibco BRL, Carlsbad, CA, USA) supplemented with 10% heat-inactivated fetal bovine serum, and 1% penicillin and streptomycin. The MCF-7 cells were maintained in Dulbecco's modified Eagle's medium supplemented with 5% fetal bovine serum, 1% penicillin and streptomycin, 4.5 g L^{-1} glucose, 0.005 mg mL^{-1} insulin, and 20 mM HEPES. Cells were cultured in tissue culture flasks (Corning, New York, NY, USA) and kept in an incubator at 37 °C in a humidified atmosphere with 5% CO$_2$. For experimental purposes, cells in the exponential growth phase (approximately 70–80% confluence) were used.

Cell imaging and MTT cell viability assay

For cell imaging, 100 μL of CDs (100 μg mL^{-1}) were incubated with MCF-7 and SH-SY5Y (Human neuroblastoma) cells (seeded at 5×10^5 mL^{-1}) for 2 h at 37 °C. In another batch, MCF-7 cells were treated with 100 μL of boldine-loaded CDs, washed three times with DMSO and then fixed with paraformaldehyde (2%).

The cytotoxic effect of blank CDs, free boldine and boldine-loaded CDs was assessed using the MTT cell viability assay. The assay was performed at different treatment time points. Briefly, 8.0×10^3 cells were seeded in a 96-well plate and incubated overnight at 37 °C in 5% CO$_2$. The following day, the cells were treated with blank CDs (100 μg mL^{-1}), free boldine (327.3 μg mL^{-1}) and boldine-loaded CDs, and incubated further at 37 °C in 5% CO$_2$. The MTT solution was added at 2 mg mL^{-1} for 2 hours before the addition of dimethylsulfoxide to dissolve the formazan crystals. After this, the medium was replaced with 200 mL of DMSO. This complex mixture was agitated slowly to dissolve the formazan crystals. Finally, the mixture was transferred into fresh 96-well plates and analyzed using a microplate reader (Thermo, USA) at 570 nm. The cell viability was calculated using the following formula (OD, optical density):

$$\text{Cell viability (\%)} = (A_{570} - A_{630}) \text{ treated cells}/(A_{570} - A_{630}) \text{ controlled cells} \times 100$$

Drug uptake studies

Confocal fluorescence microscopy was used to evaluate the boldine drug uptake from boldine-loaded CDs by the MCF-7 cells. First, cells (1×10^5) were seeded on glass coverslips and cultured for 24 hours with normal culture medium. Then, the culture medium was replaced with culture medium containing blank CDs, free boldine and boldine-loaded CDs, with boldine concentration of 327.3 μg mL^{-1}. After incubation for different times, the glass cover slips were washed three times with PBS, and subjected to fluorescence imaging at excitation wavelengths of 405, 488, and 561 nm. The amount of internalized particles in MCF-7 cells was evaluated based on the mean fluorescent intensity of blank CDs, and boldine-loaded CDs that were internalized by the MCF-7 cells.

Instrumentation

Transmission electron microscopy (TEM) images were obtained on a JEOL 2100 transmission electron microscope. Fluorescence spectra were collected using a Cary Eclipse Fluorescence Spectrophotometer (Agilent Technologies). The hydrodynamic diameter of the CDs was measured with a Malvern Zetasizer NanoZS-90 instrument at 25 °C. UV-visible spectra were obtained on a Maya Pro 2000 spectrophotometer (Ocean Optics, USA). Fourier transform infrared (FT-IR) spectra were recorded on a Perkin Elmer (FT-IR spectrum BX, Germany). The fluorescence lifetimes of the samples were recorded on a Horiba Jobin Yvon IBH Fluorocube instrument after excitation using a 370 nm picosecond diode laser. Cell images were measured using a Carl Zeiss 510 LSM laser scanning confocal microscope.

Results and discussion

Characterization of CDs

The fluorescent N-doped CDs were synthesized from dried shrimp by hydrothermal treatment at 170 °C for a period of 12 h. The TEM image and size distribution of as-prepared CDs are shown in Fig. S1 in ESI.‡ The synthesized CDs were well dispersed in water and had a spherical shape with an average diameter of ~6 nm (Fig. S2 in ESI‡). The CDs consist of carbon, nitrogen, and oxygen, which was confirmed by EDX spectroscopy (Fig. S2 in ESI‡). The elemental analysis shows the carbon, oxygen and nitrogen weight contents of CDs, implying that the heteroatoms are doped into the CDs. Furthermore, other elemental (S and P) peaks were observed in the SEM/EDX spectrum of CDs, indicating that the other elements were also present in the carbon framework. According to the reports,[40,41] elemental doping of the CDs improves either fluorescence properties or surface structures, which facilitate the tuning of the intrinsic properties of CDs for unexpected non-linear optical properties and applications.[42] Therefore, the presence of other elements may not negatively affect the fluorescence properties of the CDs. Fig. S3a in ESI‡ shows the FT-IR spectrum of blank CDs. The absorption bands at 1621 and 1402 cm^{-1} correspond to asymmetric and symmetric stretching vibrations of the carboxyl group. The band at 1675 cm^{-1} is attributed to the stretching vibration of C=O groups. The broad bands at 3200–

3600 cm^{-1} correspond to bending vibrations of the O–H group, indicating that the prepared CDs exhibit hydrophilicity, which improves their stability and dispersibility in water, without any further surface passivation.[43] The absorption band at 2879 cm^{-1} results from –CH$_2$ vibrations in the CDs. The band at 1124 cm^{-1} originates from –CH$_2$ stretching vibration deformation. The characteristic absorption band of the C–O stretching vibration mode was observed at 1047 cm^{-1}. The bands at 1562 and 1477 cm^{-1} are assigned to asymmetric and symmetric bending of primary amines (–NH$_2$), respectively, while the characteristic absorption bands at 3289 and 1337 cm^{-1} belong to the stretching vibrations of N–H and C–N groups. The presence of multifunctional groups (–COOH, –OH, C=O, and NH$_2$) on the surfaces of CDs demonstrate that the N-doped CDs were derived by the decomposition of various organic compounds in dried shrimp, resulting in the creation of a series of emissive traps with tunable emission of the CDs.

Fig. 1 shows the UV-visible absorption and fluorescence emission spectra of as prepared CDs. It can be observed that the absorption maximum occurs around 321 nm, which is due to the $\pi \rightarrow \pi^*$ transition of C=C and n $\rightarrow$ π^* transition of C=O in the CDs. In the fluorescence emission spectrum, a strong fluorescence emission peak centered at 475 nm is observed, which was obtained under excitation at 430 nm. Importantly, it can also be noticed that the as-prepared CDs are stable and exhibit a blue color under UV illumination (365 nm, inset). They also display an excellent aqueous dispersibility. In order to investigate the optical properties of the CDs, fluorescence emission spectra of the CDs were measured under various excitations. As shown in Fig. 2, with the increase in excitation wavelength from 360 to 530 nm, emission peaks are red-shifted from 430 (blue) to 543 nm (green), while the fluorescence emission intensities decrease remarkably, indicating that the excitation-dependent emissions are general features of CDs.

These results indicate that the excitation-dependent fluorescence emission behavior of the N-doped CDs results from the presence of particles of different sizes and the distribution of different surface states of the CDs.[39,44] The fluorescence quantum yield of the CDs was 54% (measured using quinine sulfate as a reference), and was comparable to those of the reported methods in the literature.[27–29] It is clear that the fluorescence emission intensity of the N-doped CDs is strong, and the fluorescence quantum yield of CDs is greatly improved at excitation wavelength of 430 nm. The decay times of the N-doped CDs in water are similar to those of other N-doped CDs in water.[39,44–46] The fluorescence lifetime (t) of as-prepared CDs was assessed by time-resolved photoluminescence measurements, and was calculated to be 7.53 ns, according to the fluorescence decay profile. Excitation and emission were monitored at 430 and 475 nm, respectively (ESI of Fig. S4‡). The CDs exhibited a short luminescence lifetime, which is indicative of radiative recombination of the excitons.[44,45]

Study of boldine loading on CDs and its release

The loading of boldine on the surfaces of CDs was assessed via UV-visible and fluorescence spectroscopic techniques, taking advantage of the spectral resolution of the absorption and emission peaks of the CDs as well as absorption spectra of the boldine-loaded CDs. The blank CDs, free boldine and boldine-loaded CDs exhibited characteristic absorption peaks at 307, 321 and 316 nm, respectively (Fig. 3). These results indicated that the boldine was effectively attached on the surfaces of the CDs. The amount of loaded boldine was determined with the help of UV-visible absorption spectra of boldine-loaded CDs at different volume ratios (boldine : CDs, 0 : 10–10 : 0, v/v) (ESI of Fig. S5‡); the amount of boldine contained within boldine-loaded CDs was 140.3 μg mL^{-1}. The fluorescence emission spectra of boldine-loaded CDs also supported this conclusion (ESI of Fig. S6‡). When the boldine-loaded CDs at different
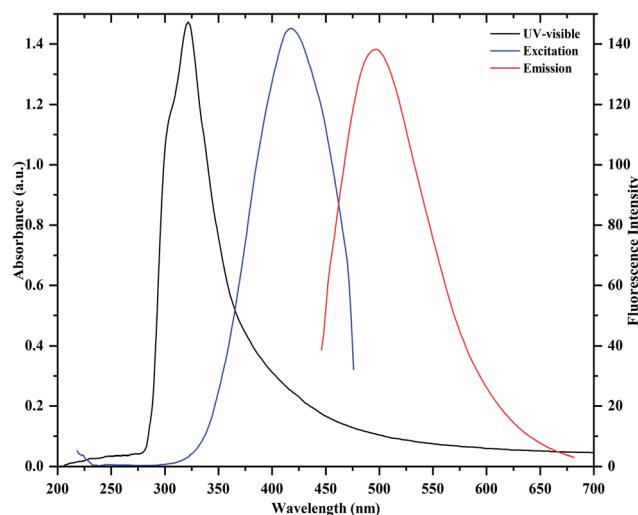

Fig. 1 UV-visible absorption spectrum and fluorescence excitation and emission spectra of CDs. Excitation and emission wavelengths are 430 nm and 475 nm, respectively. Inset picture shows the CDs under daylight (left) and UV light at 365 nm wavelength (right).
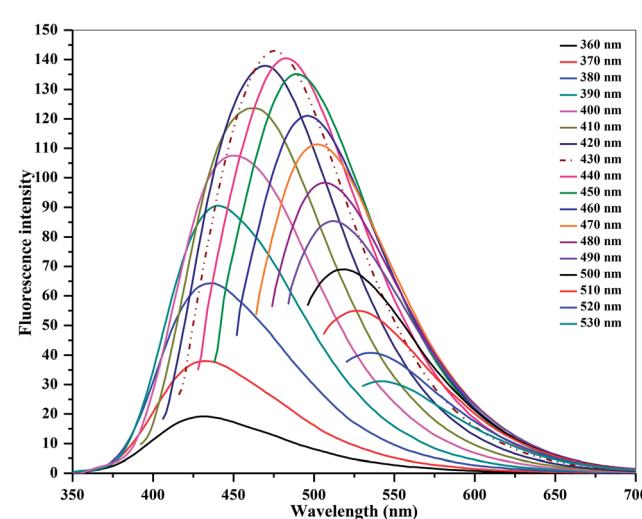

Fig. 2 Emission spectra of carbon dots at different excitation wavelengths from 360 to 530 nm, with the wavelength progressively increasing by 10 nm.
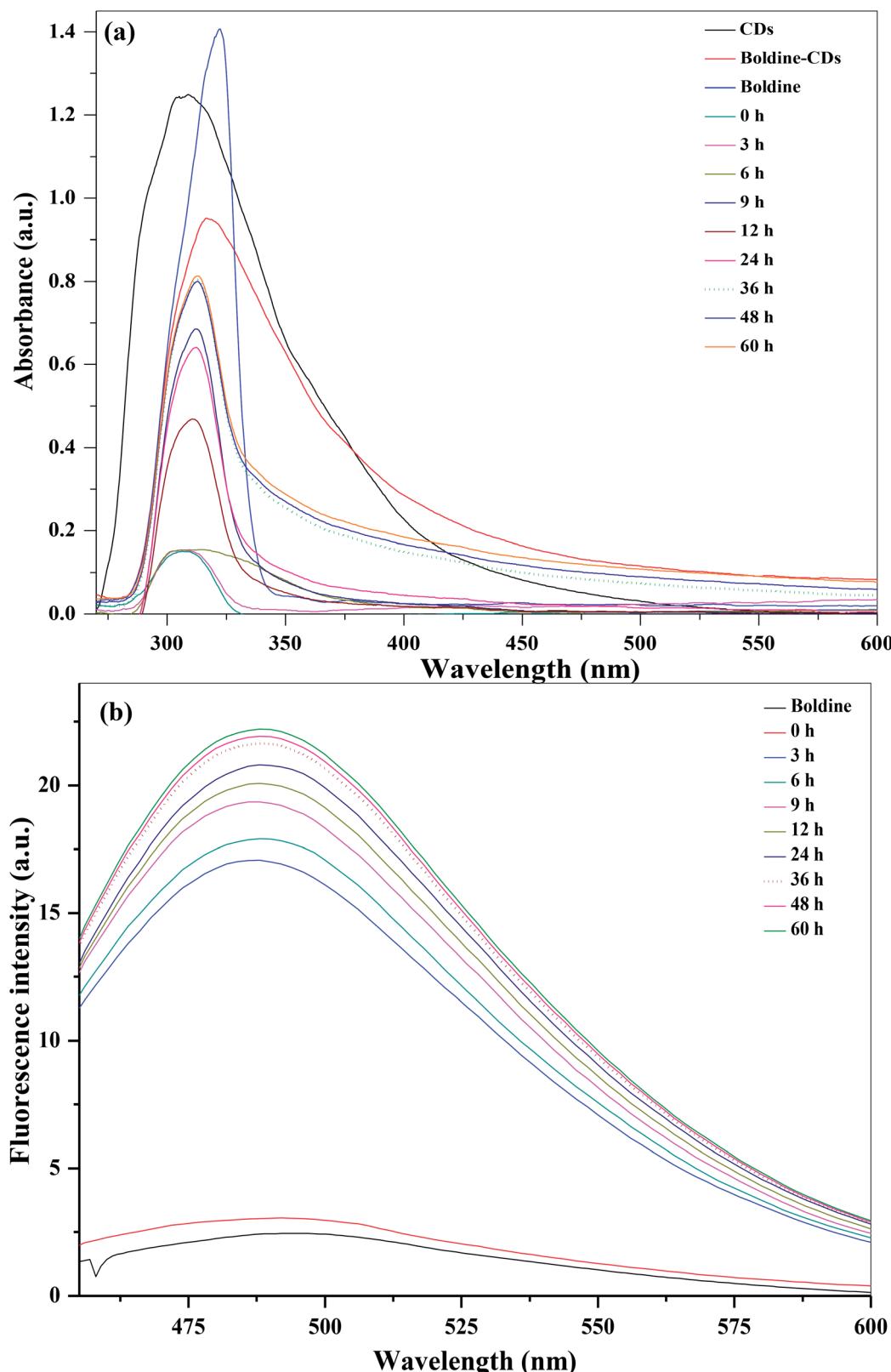
Fig. 3 (a) UV-visible and (b) emission spectra of boldine-loaded CDs at different time intervals from 0 to 60 h in PBS buffer at pH 5.2. Boldine responses for 327.27 µg mL^{-1} boldine-loaded CDs under 430 nm excitation.

volume ratios (0 : 10–10 : 0, v/v) were excited at 430 nm, there was a drastic change in the emission spectra at 475 nm corresponding to the CDs (ESI of Fig. S6‡), indicating the attachment of boldine on the surfaces of the CDs. Similarly, the UV-visible absorption spectra of boldine-loaded CDs changed drastically with varying the volume of CDs and boldine. As a result, the characteristic peaks at 308 (CDs) and 319 nm (boldine) disappeared and new peaks at 315 nm were observed at boldine and CDs ratio of 7 : 3 v/v, indicating the successful loading of boldine on the surfaces of CDs. These results provide a basis for the simultaneous tracking of the drug carriers on their way into cells, and the drug release behavior of the carriers inside the cells.

To confirm the attachment of boldine on the surfaces of CDs, we studied the FT-IR spectra of free boldine and boldine-loaded CDs. As shown in Fig. S3b of ESI,‡ the band at 3099 cm^{-1} corresponds to the sp^3 C–H stretching of boldine. The typical bands at 1499, 1514, 1582 and 1596 cm^{-1} are ascribed to the aromatic C=C stretching. The bands in the range of 1380 to 1470 cm^{-1} are ascribed to aliphatic CH deformation modes. The bands at 1385 and 1468 cm^{-1} represent CH$_3$ deformation modes. The stretching modes of the N–CH$_3$ group were observed in the range 1274–1415 cm^{-1}. The typical bands at 892, 1015 and 1630 cm^{-1} correspond to –CH bends of aromatic rings, C–N stretching and C=C stretching, respectively. The band at 3398 cm^{-1} corresponds to –OH stretching. Phenolic vibration of boldine was observed at 1206 cm^{-1} while the ether function (CH$_3$–O–Phe) stretching was observed at 1082, 1132, 1174 and 1239 cm^{-1}. The medium bands at 771, 813, 869, 892 and 983 cm^{-1} are ascribed to out of plane CH modes. The Phe–OH deformation mode was observed at 6098 cm^{-1} and the band at 564 cm^{-1} is most likely as a result of the deformation mode of the Phe–O–CH$_3$ moiety. All the observed absorption bands represent the typical molecular signatures of boldine. In Fig. S3c of ESI,‡ the FT-IR spectrum of boldine-loaded CDs, showed spectral variation, compared to the spectra of blank CDs and free boldine, which confirms the interactions of boldine with CDs. The broad band in the range of 3297–3427 cm^{-1} corresponds to the intramolecular hydrogen-bonding between CDs and boldine. It can also noticed that the O–H in-plane bending vibrations for phenolic groups lie in the region 1150–1250 cm^{-1} and are not much affected due to hydrogen bonding. The slight shift in the bands at 1458, 1507, 1576 and 1600 cm^{-1} is due to the aromatic C=C stretching resulting from the interaction of boldine with CDs. The broad peak in the range of 3169–3305 indicates the involvement of the amine group of CDs with boldine, through hydrogen bonding. These results indicate that boldine was successfully bound to the surface of CDs by non-covalent interactions.

The pH of the cytosol was ∼7.4, whereas the endocytic vesicles, where the particles were entrapped upon internalization, had a lower pH of 4.5–5.50.[46] *In vivo* applications are envisaged, and some tumors are characterized by a slightly more acidic environment than healthy tissue or blood.[47] The pH of the solution therefore plays a key role in the release of drugs from the surface of nanoparticles, and acts as a trigger for the controlled release of drugs. The boldine-loaded CDs were

dialyzed in PBS (pH 5.2, 7.4 and 9.2) for 60 hours to remove unloaded boldine. The percentage release of boldine from the CDs was determined with the help of a calibration curve at various PBS pH conditions (pH 5.2, 7.4 and 9.2), mimicking the environment of intracellular vesicles or the cytosol, respectively (Fig. 4). At these pH values, there was a continuous release with time and a plateau was reached after 36 hours (Fig. 4). At physiological pH (7.4), the percentage of drug release increased slowly, reaching a maximum value of 84.4%. At pH 5.2, the percentage of drug release significantly increased with time, to a maximum value of 84.8% after 36 hours, which was greater than that of physiological pH. These can be explained by the following. The hydrophilicity and solubility of boldine increased at pH 5.2 and different degrees of hydrogen-bonding interaction can be created between boldine and the CDs under different pH conditions.[48] In acidic conditions, the hydrogen-bonding interactions between the H$^+$ in the solution and the –COOH, –OH, and –NH$_2$ groups of the CDs and the –OH groups of boldine are weaker than those occurring at neutral pH. At pH 7.4, the phenolic groups of boldine show high affinity for interaction with the protonated groups of the CDs (NH$_3^+$), and exhibit a negative charge since boldine has a pK_a of 6.90,[49] which inhibits its release from the CDs surfaces. Thus, there is the possibility of using pH as an internal trigger for releasing boldine from the surfaces of the CDs.

As shown in Fig. 3, UV-visible absorption and fluorescence emission spectra of boldine-loaded CDs exhibit different spectral characteristics at different time intervals from 0 to 60 h. A dialysis membrane was used against a buffer solution. Fig. 3a shows the UV-visible absorption spectra of the kinetics of boldine release from the CDs surfaces at different time intervals at pH 5.2. It can be observed that the intensity of the absorption peak at 312 gradually increased with time, and reached to a maximum at 36 hours. Similarly, the fluorescence emission intensity of the CDs at 491 nm steadily increased with increasing time, and the maximum percentage of drug release was reached at 36 hours, confirming the complete release of
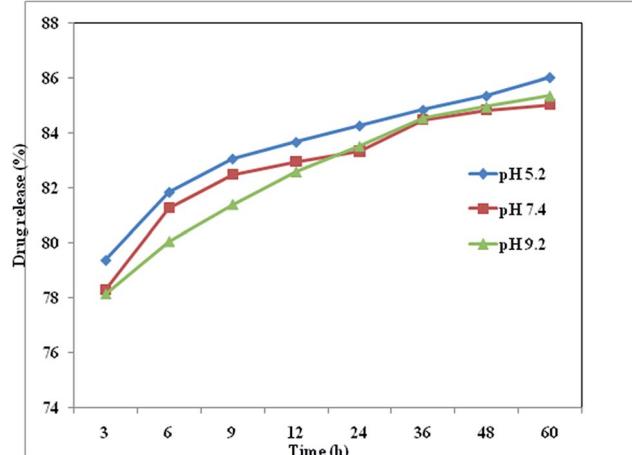
Fig. 4 Boldine drug release (%) from boldine-loaded CDs in PBS with pH values of 5.2, 7.4 and 9.2 at 37 °C.

boldine drug on the surfaces of CDs, which restores the fluorescence emission properties of the CDs (Fig. 3b). Various statistical models including the zero order, primary order, Higuchi, Hixson–Crowell, Baker–Lonsdale, Wibull, Hopenfenburg, and sequential layer models, have been used for the explanation of drug release kinetics. The present boldine drug release mechanism follows the Hixson–Crowell model, since the drug release mechanisms may depend on the nature of the materials, and the diameter and surface area vary, which is in good agreement with the reported method in the literature using carbon dots as dopamine drug carriers.[50,51] Based on the above results, the CDs act as efficient carriers to accomplish the release and accumulation of drugs in targeted tumor tissues.

Biocompatibility and cellular uptake of boldine-loaded CDs

The potential applications and the toxicity of the as-synthesized CDs were evaluated in MCF-7 cells by laser scanning confocal microscopy. Since the objective of the present study was to develop a CD platform to deliver therapeutics to tumors, preliminary studies were carried out to ascertain the suitability of CDs as imaging and delivery probes for MCF-7 cells. Fig. 5a shows the confocal microscopy images of MCF-7 cells incubated with bare CDs for 3 and 48 h at 37 °C. Under 405, 488 and 543 nm excitation, blue, green and red fluorescence of bare CDs in the cell cytoplasm was observed, respectively, using a laser scanning confocal microscope. The MCF-7 cells showed high uptake of bare CDs; most of the CDs got into the cell nucleus through nuclear pores, lightening the whole cell. When excited under different wavelengths, blue, green and red photoluminescence was found in the entire cell cytoplasm, indicating that the bare CDs were effectively taken up by the MCF-7 cells and mainly localized in the cytoplasm, instead of entering the nucleus. The images of MCF-7 cells show different colored emissions, which has roots in the excitation dependent luminescence of the CDs. Importantly, the fluorescence intensity of CDs in the cells was almost same, even after 48 h (Fig. 5b),
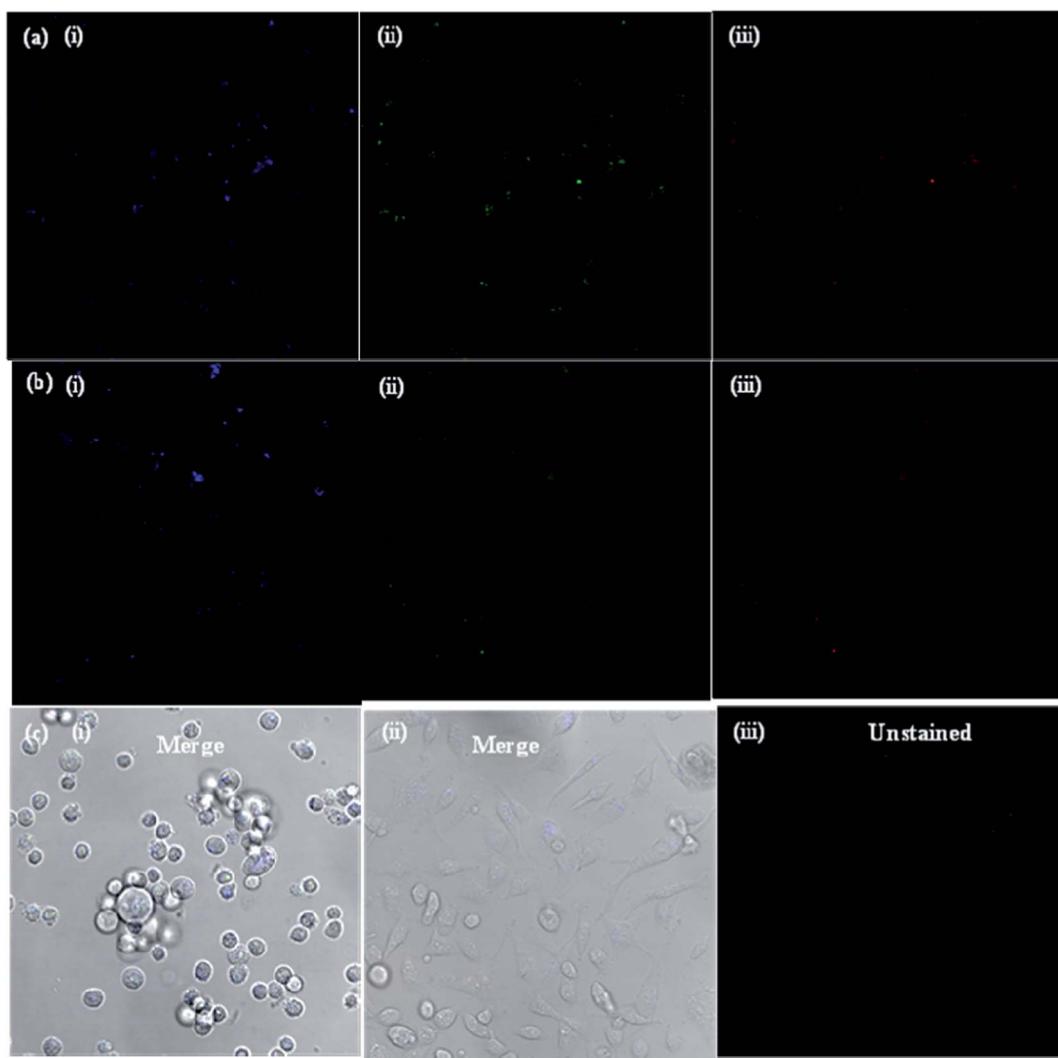
Fig. 5 Localization of bare CDs in MCF-7 cells. The cells were incubated with bare CDs for (a) 0 and (b) 48 h at 37 °C. The images were obtained under different laser excitations of (i) 405 nm; (ii) 488 nm; and (iii) 561 nm. (c) Localization of bare CDs in MCF-7 cells in merge mode at (i) 0 h, (ii) 48 h and (iii) unstained (without CDs).

indicating that the CDs are stable and exhibit strong fluorescence properties for a long time. These results indicate that the CDs show good biocompatibility as bioimaging agents and can act as imaging probes.

The drug delivery capability of boldine-loaded CDs was also investigated by the uptake behavior in MCF-7 cells. Once the uptake of CDs, the localization in acidic vesicles, and the use of pH as a trigger for the release of boldine from the CDs was established, the performance of the CD-based drug delivery system was evaluated *in vitro* in the MCF-7 cell lines. To this end, MCF-7 cells were exposed to boldine-loaded CDs at 24 and 48 h. As shown in Fig. 6, very weak fluorescence signals were observed in the cellular uptake of boldine-loaded CDs at 24 h under laser excitations of 405, 488, and 561 nm. The MCF-7 cells incubated with boldine-loaded CDs for 48 h exhibited good fluorescence signals, suggesting the effective uptake of boldine-loaded CDs by MCF-7 cells through receptor-mediated endocytosis.[31–35] Blue, green and red fluorescence was clearly visible at

48 h, which is indicative of boldine drug entering into cells quickly, *via* a membrane diffusion pathway and accumulating in the nuclei after incubation. As a result, boldine from boldine-loaded CDs could reach to the nuclei of MCF-7 cells with increasing time, while the CDs were still outside of the cell nuclei, suggesting that the boldine was released from the boldine-CDs. After 48 hours of incubation, more boldine was distributed in the cell nuclei, indicating that more boldine was released from the boldine-CDs and penetrated into the cell nuclei. These results confirm the pH-mediated release of the drug[46] from the entrapped acidic vesicles (where the CDs were) to the cytosol, and its diffusion to the target site, the nucleus. As a result, non-covalent interactions (hydrogen bonding) were weakened in the extracellular fluids of the tumor, which facilitated the release of more boldine from boldine-CDs within the cells. Therefore, fluorescence could be observed in the cells due to the cellular uptake of boldine-CDs by the MCF-7 cells *via* endocytosis, along with the gradual intracellular release of
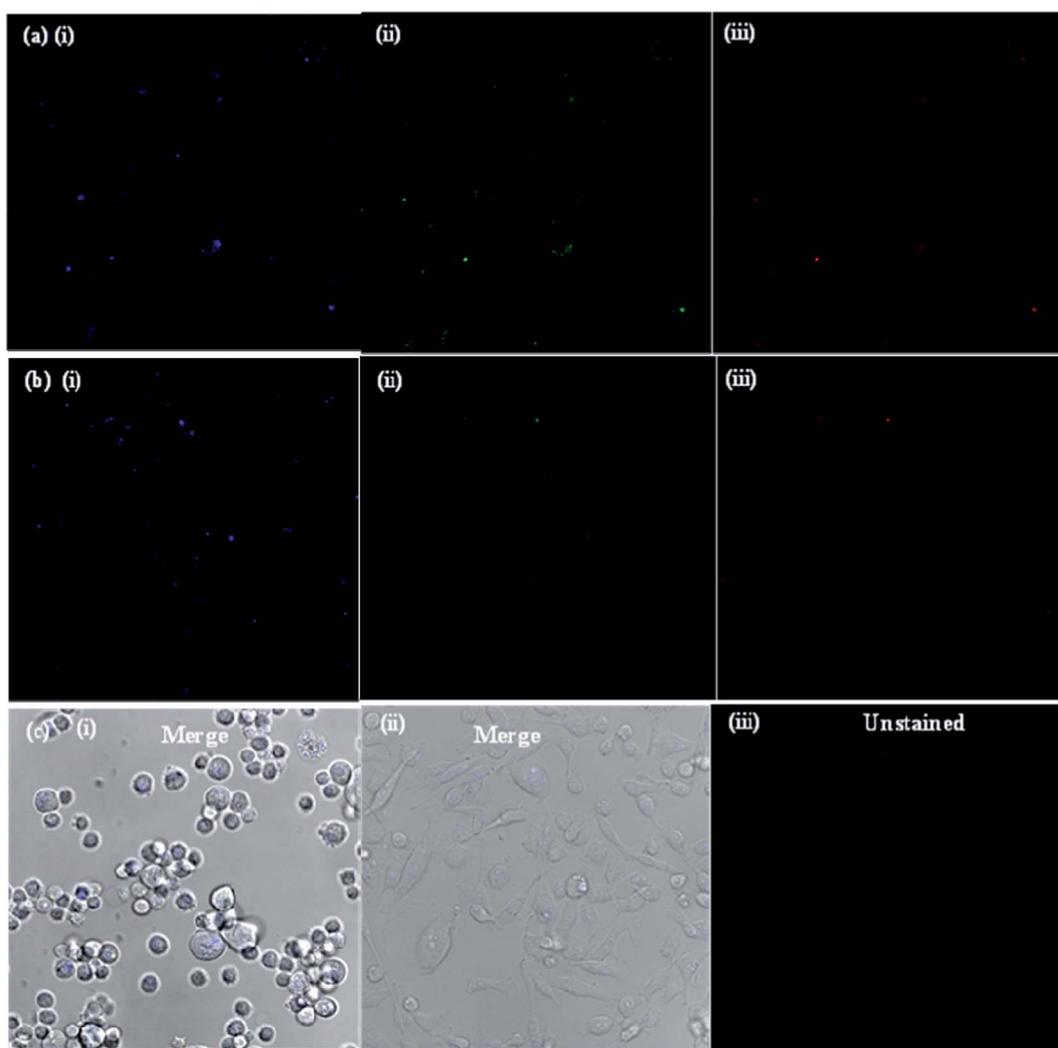
Fig. 6 Laser scanning confocal microscopy images showing the cellular uptake of boldine–CDs by MCF-7 cells at (a) 24 h and (b) boldine–CDs at 48 h, obtained under different laser excitations of (i) 405 nm; (ii) 488 nm; (iii) 561 nm. (c) Localization of boldine–CDs in MCF-7 cells in merge mode at (i) 0 h, (ii) 48 h and (iii) unstained (without boldine–CDs).

Fig. 7 Laser scanning confocal microscopy images of SH-SY5Y (human neuroblastoma) cells after the cellular uptake of CDs.

In order to prove that the as-synthesized CDs could act as universal imaging probes for all cell lines, the SH-SY5Y (human neuroblastoma) cell uptake of the blank CDs, and bioimaging experiments were performed using a confocal fluorescence microscope *in vitro*. As shown in Fig. 7, the morphologies of SH-SY5Y (human neuroblastoma) cells are almost unchanged before and after incubation with the blank CDs, further confirming their good biocompatibility and low toxicity. The bright blue and green areas inside the SH-SY5Y cells can be clearly observed after excitation at 405 and 488 nm, indicating that the CDs are easily internalized by the cells, which suggests that the CDs are stable. Notably, the fluorescent spots are observed in the cells, and indicate that the CDs easily penetrate the cells but are only in the cytoplasm. All of the above results show that the CDs are indeed suitable for long time cell imaging. The excellent biocompatibility (low cytotoxicity) of the CDs guarantees the practical applications as carriers in drug delivery for human beings.

In vitro cytotoxicity

In vitro cytotoxicity studies of blank CDs, free boldine and boldine-loaded CDs were performed on the MCF-7 cells by MTT assay. The MCF-7 cells were incubated with blank CDs, boldine-loaded CDs and free boldine at 10, 100, 250 and 500 µg mL^{-1}, for 24, 48, and 72 h each. It was observed that all formulations of free boldine inhibited the growth of MCF-7 cells in both a time-dependent and dose dependent manner. The blank CDs at 10 µg mL^{-1} did not cause obvious cytotoxicity against MCF-7 cells even at 72 h incubation. It was also noticed that there was similar cytotoxicity in MCF-7 cells for boldine-loaded CDs (10 µg mL^{-1}) at 24 h incubation. The viability of MCF-7 cells after 24 h

boldine from boldine-loaded CDs in the acidic micro-environment of the MCF-7 cells. These changes can enhance the drug concentration in the cells, thereby improving drug cytotoxicity. The boldine-CDs drug delivery system steadily released boldine, translocated it away from the CDs and moved it into the nucleus, indicating that CDs act as ideal carrier probes for the simultaneous treatment and tracking of cancer cells.

Fig. 8 Relative cell viabilities of MCF-7 cells incubated with blank CDs, boldine-CDs and free boldine at 10, 100, 250 and 500 µg mL^{-1} for 24, 48 and 72 h.

contact with 10, 100, 250 and 500 $\mu g\ mL^{-1}$ blank CDs was 104%, 47%, 10% and 6% respectively, whereas for cells treated with boldine-loaded CDs, it was 102%, 24%, 9% and 8% respectively, while for cells treated with free boldine drug, it was 101%, 8%, 8% and 10% respectively. As shown in Fig. 8, the blank CDs were found to have no obvious effect on the viability of MCF-7 cells. However, the MCF-7 cells were significantly damaged after incubation with boldine-loaded CDs. For a boldine concentration of 327.3 $\mu g\ mL^{-1}$, boldine molecules delivered into the nucleus by boldine-CDs showed more severe cytotoxicity to MCF-7 cells, indicating that boldine-CDs are more readily internalized through the receptor-mediated endocytosis mechanism, while free boldine is transported into cells by a passive diffusion mechanism. As shown in Fig. 8, the boldine-loaded CDs induced death in MCF-7 cells at a comparable rate to free boldine, indicating that the loaded boldine retained its pharmaceutical activity, and caused minimal side effects to the normal cells.

Conclusions

In this study, we report a facile hydrothermal approach for the synthesis of highly fluorescent N-doped CDs using dried shrimps as precursors. The synthesized CDs have multifunctional groups (amino, carboxylic acid and hydroxyl) that can easily facilitate the loading of boldine on the surfaces of the CDs *via* hydrogen bonding. The fluorescent N-doped CDs act as new fluorescent probes that simultaneously facilitate the imaging/mapping of MCF-7 and SH-SY5Y (human neuroblastoma) cells and act as carriers for the delivery of boldine drug to the target cells. The multifunctional groups on the CDs provide excellent stability, in addition to attractive fluorescence and extremely high drug loading efficiency. The blank CDs exhibit low cytotoxicity, and only a minute amount is required for effective diagnostic and therapeutic applications. Confocal fluorescence images showed the internalization of boldine by endosomes, wherein boldine was efficiently released and entered the cell nucleus and induced MCF-7 cell death, which is indicative of the effectiveness and selectivity of the drug carrier system. These results demonstrate that the fluorescent N-doped CDs act as fluorescent probes as well as drug carriers for imaging and selective target delivery, indicating that the biocompatible CDs hold great promise for personal drug delivery with maximal pharmaceutical effects and reduced side effects in chemotherapy.

Acknowledgements

References

1 C. E. DeSantis, C. C. Lin, A. B. Mariotto, R. L. Siegel, K. D. Stein, J. L. Kramer, R. Alteri, A. S. Robbins and A. Jemal, *Ca-Cancer J. Clin.*, 2014, **64**, 252–271.

2 A. B. Chinen, C. M. Guan, J. R. Ferrer, S. N. Barnaby, T. J. Merkel and C. A. Mirkin, *Chem. Rev.*, 2015, **115**, 10530–10574.

3 World Health Organization, 2014, www.who.int.

4 S. E. Atawodi, *Infect. Agents Cancer*, 2011, **6**, 2–S9.

5 A. Jemal, R. Siegel, E. Ward, T. Murray, J. Xu and M. J. Thun, *Ca-Cancer J. Clin.*, 2007, **57**, 43–66.

6 M. Paydar, B. Kamalidehghan, Y. L. Wong, W. F. Wong, C. Y. Looi and M. R. Mustafa, *Drug Des., Dev. Ther.*, 2014, **8**, 719–733.

7 R. Scatena, *Adv. Exp. Med. Biol.*, 2012, **942**, 287–308.

8 T. Verfaillie, A. D. Garg and P. Agostinis, *Cancer Lett.*, 2013, **332**, 249–264.

9 R. Suzuki, Y. Yasui, H. Kohno, S. Miyamoto, M. Hosokawa, K. Miyashita and T. Tanaka, *Oncol. Rep.*, 2006, **16**, 989–996.

10 H. Speisky and B. K. Cassels, *Pharmacol. Res.*, 1994, **29**, 1–12.

11 P. O'Brien, C. Carrasco-Pozo and H. Speisky, *Chem.-Biol. Interact.*, 2006, **159**, 1–17.

12 D. Gerhardt, A. P. Horn, M. M. Gaelzer, R. L. Frozza, A. Delgado-Cañedo, A. L. Pelegrini, A. T. Henriques, G. Lenz and C. Salbego, *Invest. New Drugs*, 2009, **27**, 517–525.

13 D. Gerhardt, G. Bertola, F. Dietrich, F. Figueirz, A. Zanotto-Filho, J. C. Moreira Fonseca, F. B. Morrone, C. H. Barrios, A. M. Battastini and C. G. Salbego, *Urol. Oncol.*, 2014, **32**, 36e1–36e9.

14 O. C. Farokhzad and R. Langer, *ACS Nano*, 2009, **3**, 16–20.

15 S. Laurent, D. Forge, M. Port, A. Roch, C. Robic, L. V. Elst and R. N. Muller, *Chem. Rev.*, 2008, **108**, 2064–2110.

16 S. Parveen, R. Misra and S. K. Sahoo, *Nanomedicine: Nanotechnology, Biology and Medicine*, 2012, **8**, 147–166.

17 L. Li, B. Yu and T. You, *Biosens. Bioelectron.*, 2015, **74**, 263–269.

18 Y. Li, Y. Zhao, H. Cheng, Y. Hu, G. Shi, L. Dai and L. Qu, *J. Am. Chem. Soc.*, 2011, **134**, 15–18.

19 J. Przepiorsi, M. Skrodzewicz and A. W. Morawski, *Appl. Surf. Sci.*, 2004, **225**, 235–242.

20 B. Jurgens, E. Irran, J. Senker, P. Kroll, H. Muller and W. Schnick, *J. Am. Chem. Soc.*, 2003, **125**, 10288–10300.

21 J. S. Lee, X. Wang, H. Luo, G. Baker and S. Dai, *J. Am. Chem. Soc.*, 2009, **131**, 4596–4597.

22 Y. Xu, M. Wu, Y. Liu, X.-Z. Feng, X.-B. Yin, X.-W. He and Y.-K. Zhang, *Chem.–Eur. J.*, 2013, **19**, 2276–2283.

23 W. Wang, Y. C. Lu, H. Huang, J. J. Feng, J. R. Chen and A. J. Wang, *Analyst*, 2014, **139**, 1692–1696.

24 Q. Q. Shi, Y. H. Li, Y. Xu, Y. Wang, X. B. Yin, X. W. He and Y. K. Zhang, *RSC Adv.*, 2014, **4**, 1563–1566.

25 X. Sun, C. Brückner and Y. Lei, *Nanoscale*, 2015, **7**, 17278–17282.

26 M. Xu, S. Xu, Z. Yang, M. Shu, G. He, D. Huang, L. Zhang, L. Li, D. Cui and Y. Zhang, *Nanoscale*, 2015, **7**, 15915–15923.

27 V. N. Mehta, S. Jha and S. K. Kailasa, *Mater. Sci. Eng., C*, 2014, **38**, 20–27.

28 V. N. Mehta, S. Jha, H. Basu, R. K. Singhal and S. K. Kailasa, *Sens. Actuators, B*, 2015, **213**, 434–443.

29 V. N. Mehta, S. Jha, R. K. Singhal and S. K. Kailasa, *New J. Chem.*, 2014, **38**, 6152–6160.

30 B. S. B. Kasibabu, S. L. D'souza, S. Jha, R. K. Singhal, H. Basu and S. K. Kailasa, *Anal. Methods*, 2015, **7**, 2373–2378.

31 A. Mewada, S. Pandey, M. Thakur, D. Jadhav and M. Sharon, *J. Mater. Chem. B*, 2014, **2**, 698–705.

32 L. Zhou, Z. Li, Z. Liu, J. Ren and X. Qu, *Langmuir*, 2013, **29**, 6396–6403.

33 I. Matai, A. Sachdev and P. Gopinath, *ACS Appl. Mater. Interfaces*, 2015, **7**, 11423–11435.

34 B. Wang, S. Wang, Y. Wang, Y. Lv, H. Wu, X. Ma and M. Tan, *Biotechnol. Lett.*, 2015, **26**, 1–11.

35 H. Ding, F. Du, P. Liu, Z. Chen and J. Shen, *ACS Appl. Mater. Interfaces*, 2015, **7**, 6889–6897.

36 S. Pandey, M. Thakur, A. Mewada, D. Anjarlekar, N. Mishra and M. Sharon, *J. Mater. Chem. B*, 2013, **1**, 4972–4982.

37 S. Karthik, B. Saha, S. K. Ghosh and N. D. Pradeep Singh, *Chem. Commun.*, 2013, **49**, 10471–10473.

38 E. Song, W. Han, C. Li, D. Cheng, L. Li, L. Liu, G. Zhu, Y. Song and W. Tan, *ACS Appl. Mater. Interfaces*, 2014, **6**, 11882–11890.

39 C. Núñez, E. Oliveira, J. García-Pardo, M. Diniz, J. Lorenzo, J. L. Capelo and C. Lodeiro, *J. Inorg. Biochem.*, 2014, **137**, 115–122.

40 J. Liu, X. Liu, H. Luo and Y. Gao, *RSC Adv.*, 2014, **4**, 7648–7654.

41 Y. Chen, Y. Wu, B. Weng, B. Wang and C. Li, *Sens. Actuators, B*, 2016, **223**, 689–696.

42 A. Sachdev, I. Matai and P. Gopinath, *RSC Adv.*, 2014, **4**, 20915.

43 M. Algarra, B. B. Campos, K. Radotić, D. Mutavdžić, T. J. Bandosz, J. Jiménez-Jiménez, E. Rodriguez-Castellon and J. C. G. Esteves da Silva, *J. Mater. Chem. A*, 2014, **2**, 8342.

44 D. Wang, X. Wang, Y. Guo, W. Liu and W. Qin, *RSC Adv.*, 2014, **4**, 51658–51665.

45 Y. Q. Zhang, D. K. Ma, Y. Zhuang, X. Zhang, W. Chen, L. L. Hong, Q. X. Yan, K. Yub and S. M. Huang, *J. Mater. Chem.*, 2012, **22**, 16714–16718.

46 X. Teng, C. Ma, C. Ge, M. Yan, J. Yang and Y. Zhang, *J. Mater. Chem. B*, 2014, **2**, 4631–4639.

47 P. R. Gil, M. Nazarenus, S. Ashraf and W. J. Parak, *Small*, 2012, **8**, 943–948.

48 C. Schweiger, R. Hartmann, F. Zhang, W. J. Parak, T. H. Kissel and P. R. Gil, *J. Nanobiotechnol.*, 2012, **10**, 28.

49 D. Depan, J. Shah and R. D. K. Misra, *Mater. Sci. Eng., C*, 2011, **31**, 1305–1312.

50 C. I. Cámara, C. A. Bornancini, J. L. Cabrera, M. G. Ortega and L. M. Yudi, *Talanta*, 2010, **83**, 623–630.

51 M. S. Khand, S. Pandeya, A. Talibd, M. L. Bhaisarea and H. F. Wu, *Colloids Surf., B*, 2015, **134**, 140–146.